Dalton Transactions

Accepted Manuscript

ROYAL SOCIETY OF CHEMISTRY

www.rsc.org/dalton

Structural, Raman spectroscopic and microwave dielectric studies on $Ni_{1-x}(Zn_{1/2}Zr_{1/2})_xW_{1-x}Nb_xO_4$ ceramic compounds with Wolframite structure

S.D. Ramarao and V.R.K. Murthy*

Microwave laboratory, Department of Physics, Indian Institute of Technology Madras, Chennai – 600 036

Abstract

$Ni_{1-x}(Zn_{1/2}Zr_{1/2})_xW_{1-x}Nb_xO_4$ (x = 0.0 – 1.0) compositions were synthesized via conventional solid state reaction method. Structural and lattice vibrational characteristics of these compositions were studies with help of powder X-ray diffraction and Raman spectroscopic measurements. Rietveld refinements confirm the formation of all these compositions in monoclinic Wolframite structure with P2/c space group. When we are moving towards Ni^{2+} poor compositions, splitting in the X-ray reflections was observed and is explained with lattice parameter variation. With increasing the concentration of x, Raman spectra show two additional Raman active modes and the possible reasons for observing these modes is discussed in terms of electronegativity difference of the randomly distributed cations in B-site of these compositions. X-ray Photoelectron Spectroscopic (XPS) measurements were done on these compositions to understand the chemical bonding states of different elements in these compositions. Surface morphology studies reveal that, the average grain size is increased with increasing the concentration of x. Microwave dielectric properties such as dielectric constant and quality factor were measured using Hakki-Colemann and reflection cavity technique and enhancement in these values with x concentration is correlated with intrinsic parameters such as polarizability and 3d electrons present in the constituent ions of these compositions respectively. Temperature coefficient of resonant frequency was measured using an invar cavity attached to programmable hot plate and is explained with

B-site octahedral distortion of these compositions. Well dense $Ni_{1-x}(Zn_{1/2}Zr_{1/2})_xW_{1-x}Nb_xO_4$ (x = 0.0 – 1.0) compositions possess good microwave dielectric properties.

Keywords: Wolframite structure; Rietveld refinement; Raman spectroscopy; Octahedral distortion; Microwave dielectric properties

*Corresponding author: Telephone +91-44-22574859; Fax: +91-44-22570545

1. Introduction

Dielectric ceramics such as dielectric resonators (DRs) gaining much attention in the rapid growth of mobile, satellite and radar technology because of their compact size and low-loss nature in comparison with metallic wave guides and coaxial lines and lead to the device miniaturization.[1,2] These DRs are available with different shapes such as solid cylinder, circular, tubular, spherical and parallelepiped. But in general, one can see solid cylinder and circular DRs in microwave integrated circuits.[3] Storage of microwave energy at discrete frequencies through total internal reflection at air-dielectric interface is the basic working principle of these dielectric resonators.[3] DR with higher dielectric constant (ε_r ~20) reduces the size of microwave devices and is because of the wavelength of electromagnetic wave in the dielectric material is inversely proportional to square root of dielectric constant. Enhanced the signal to noise ratio is achieved by these DRs because of their lower dielectric loss or higher quality factor (Q>3000 at 10 GHz).[1-3] Atmospheric conditions such as temperature effects the resonant frequency of these DRs which in turn influences the performance of microwave devices. The usability of microwave devices at different atmospheric conditions can be increase by tuning the temperature coefficient of resonant frequency of these DRs.[1-3] Perovskites (ABO_3), complex perovskites ($AA'BB'O_3$), cation deficient perovskites ($A_nB_{n-1}O_{3n}$) and columbites (AB_2O_6) materials were extensively studied as DRs for

microwave device applications because of flexibility for substitution of different cations in A- and B-sites for tuning the dielectric properties of these compounds.[4-7]

Recently, researchers focused on microwave dielectric properties of $A^{+2}B^{+6}O_4$ (B: Mo and W) compounds because of their lower processing temperatures and formation of these compounds in different crystallographic symmetries such as monoclinic Wolframite and tetragonal Scheelite structure.[8-10] More recently, Zhou *et al.,* reported the low temperature firing (i.e. below 850 ^oC) ceramics with ABO_4 stoichiometry.[11,12] In the scheelite structure, the rigid symmetric isolated BO_4 tetrahedra are connected AO_8 dodecahedra by corner sharing whereas the A-site dodecahedra are connected via edge sharing. On the other hand, in Wolframite structure, both A- and B-site cations connected to six oxygen atoms giving distorted AO_6 and BO_6 octahedra where the B-site octahedra are distorted more in comparison with A-site octahedra.[13] These A-site and B-site octahedra are edge shared and form zigzag chains running along z direction.[13] Ionic radius of A-site cation decides the formation of $A^{+2}B^{+6}O_4$ (B: Mo, W) compounds in either Wolframite or Scheelite structure.[13,14] Wolframite structure with P2/c space group can be obtained with substitution of divalent cations with lower ionic radius i.e. $r_A \leq 0.77$ Å (Ni, Mg, Mn, Zn and Co) at A-site whereas the $A^{2+}B^{6+}O_4$ (B: Mo and W) compounds form in Scheelite structure with $I4_1/a$ space group when the A-site occupied by larger ($r_A \geq 0.99$ Å) divalent cations such as Ca, Sr, Pb and Ba. [13,14]

Structure and microwave dielectric properties of AWO_4 (A: Mg, Zn, Mn, Ca, Sr and Ba) were reported by Yoon *et.al* where they observed higher dielectric constant values for AWO_4 (A: Mg, Zn and Mn) in spite of their lower polarizability in comparison with AWO_4 (A: Ca, Sr and Ba) compounds and was attributed to the higher molar volume of Wolframite structure than Scheelite structure.[15] Puller *et al.* reported the microwave dielectric properties

of AWO_4 (A= Mg, Zn, Ni and Co) compounds with Wolframite structure explained variation in dielectric constant and quality factor with an extrinsic parameters density.[16] As the ionic polarizability of Mo was not reported by Shanon[17], Choi *et al.* calculated the polarizability of Mo (3.28 $Å^3$) using least square refinement in conjunction with Clausius-Mosotti equation and discussed the variation in temperature coefficient resonant frequency (τ_f) of Wolframite structured $AMoO_4$ (A: Mg, Zn and Mn) with molar volume of these compounds.[18] As the octahedral distortion is indirectly related to the volume of the unit cell, Kim *et.al* explained the variation in τ_f with octahedral distortion in compounds with Wolframite structure.[19] Kim *et al.* reported that, the quality factor variation in ABO_4 compounds with Scheelite structure was correlated with their packing fraction.[14] More recently, a similar interpretation between quality factor and packing fraction was reported by Kim *et al.* in Wolframite structured ABO_4 (A: Ni, Zn and Mg and B: Mo and W) compounds where $NiWO_4$ posses lower quality factor in spite of its higher quality factor than other and explained this with presence of localized d electrons present in Ni^{2+} ($3d^8$).[20]

These reports give an idea for improving the dielectric properties Wolframite structured compounds and motivated us to synthesize low dielectric loss materials with by replacing Ni^{2+} with ions having empty or completely filled d orbital such as Zr^{4+} (d^0) and Zn^{2+} (d^{10}). In order to stability the wolframite structure through compositions we have replaced W^{6+} with Nb^{5+} and synthesized the $Ni_{1-x}(Zn_{1/2}Zr_{1/2})_xW_{1-x}Nb_xO_4$ (x = 0.0 – 1.0) compositions. In the present report we studied the structural, lattice vibrational and microwave dielectric properties of $Ni_{1-x}(Zn_{1/2}Zr_{1/2})_xW_{1-x}Nb_xO_4$ (x = 0.0 – 1.0) compositions. Rietveld refinement was performed on all these compositions to study the variation in the structural characteristics. Raman mode assignment was done for all these compositions and reasons for rising two additional modes in these compositions is explained with

electronegativity difference between the elements occupied in the same site. According to the literature, $NiWO_4$ possess very low quality factor out of all the compounds with Wolframite structure. Therefore, in the present manuscript we report the enhancement in the quality factor and dielectric constant with substitution of Zn^{2+}, Zr^{4+} at A-site and Nb^{5+} at B-site of $NiWO_4$ compounds. The possible reasons for enhancement in the microwave dielectric properties of $Ni_{1-x}(Zn_{1/2}Zr_{1/2})_xW_{1-x}Nb_xO_4$ (x = 0.0 – 1.0) compositions are explained with the intrinsic parameters such as polarizability, d electrons present in the constituent ions and B-site octahedral distortion of these compositions.

2. Experimental procedures

Conventional solid state reaction method was followed for synthesizing the $Ni_{1-x}(Zn_{1/2}Zr_{1/2})_xW_{1-x}Nb_xO_4$ (x = 0.0 – 1.0) compositions. Initial ingredients NiO (99.9%), ZnO (99.95%), ZrO_2 (99.7%), WO_3 (99.95%) and Nb_2O_5 (99.5%) were weighed with stoichiometric amounts and were ground in an agate mortar using pestle for 2 h. All these compositions were calcined in 900 – 1300 ^oC temperature range with holding time 4 h. Both heating and cooling was maintained with a rate of 5 °C/min. The obtained agglomerated powders were again ground in both dry and wet conditions in order to get fine powders. These fine powders were used for collecting the powder X-ray diffraction patterns of $Ni_{1-x}(Zn_{1/2}Zr_{1/2})_xW_{1-x}Nb_xO_4$ (x = 0.0 – 1.0) compositions using Philips PANAlytical X'pert Pro X-ray diffractometer with X'Celerator detector. We have used Cu K_α radiation at an acceleration condition of 40 kV and 30 mA. Both the incident and receiving soller slits were maintained at 0.02° whereas the divergent slit was maintained at 1° and data was collected with a scan step of 0.0169^o. Structural characteristics of $Ni_{1-x}(Zn_{1/2}Zr_{1/2})_xW_{1-x}Nb_xO_4$ (x = 0.0 – 1.0) compositions were studied with help of Rietveld refinement using GSAS suite equipped with EXPGUI software.[21,22] The initial parameters for these refinements were taken from an

article report by Daturi *et al*.[13] Cylindrical pellets of 8 mm diameter and 7 mm thickness were prepared by adding 3 wt. % poly vinyl alcohol to these powders. Uni-axial hydraulic press with a pressure of 200 MPa was used for this compaction process. All these pellets were placed on a platinum foil and sintered in 1200 – 1350 ^{o}C temperature range using conventional resistive heating furnace.

Horiba Jobin Yvon HR800 UV Raman spectrometer equipped with Peltier-cooled charge-coupled device detector was used to collect Raman spectra of polished and thermally etched $Ni_{1-x}(Zn_{1/2}Zr_{1/2})_xW_{1-x}Nb_xO_4$ (x = 0.0 – 1.0) compositions. All these measurements were done with He-Ne laser source with an excitation wavelength λ=632.8 nm and the measured output powder at the surface of the sample is about 3 mW. Chemical bonding states of the constituent elements of these compositions were determined using X-ray photoelectron spectroscopy (XPS, Omicron Nanotechnology) measurements. The bulk densities of all these sintered compositions were measured using the Archimedes technique. Surface morphology of polished and thermally etched compositions was studied with help of FEI Quanta 400 high resolution Scanning Electron Microscope. Vector Network Analyzer (PNA-L N5230C) was used to measure the microwave dielectric properties of these compositions. Dielectric constant and quality factor of $Ni_{1-x}(Zn_{1/2}Zr_{1/2})_xW_{1-x}Nb_xO_4$ (x = 0.0 – 1.0) compositions were measured using Hakki-Coleman method[23] and reflection technique whereas the temperature coefficient of resonant frequency (τ_f) of all these compositions was calculated using the following formula.

$$\tau_f = \frac{f_{85} - f_{25}}{f_{25} \times (85 - 25)} \text{ ppm/}^{o}\text{C} \qquad (1)$$

where f_{85} and f_{25} are the resonant frequencies at 85^{o}C and 25^{o}C respectively.

AC conductivity of $Ni_{1-x}(Zn_{1/2}Zr_{1/2})_xW_{1-x}Nb_xO_4$ (x = 0.0 – 1.0) compositions were measured at room temperature using LCR meter (PSM 1700 N4L).

3. Results and discussion

3.1 Structural and Raman spectroscopic studies

X-ray diffraction patterns of $Ni_{1-x}(Zn_{1/2}Zr_{1/2})_xW_{1-x}Nb_xO_4$ (x = 0.0 – 1.0) compositions are shown in Fig. 1(a) and from this we can clearly indicate that, all the X-ray reflections are shifting to lower angle side with increasing the concentration of x. With substitution of higher ionic radius[24] elements Zn^{2+} (0.74 Å), Zr^{4+} (0.72 Å) and Nb^{5+} (0.64 Å) ions in place of lower ionic radius elements Ni^{2+} (0.69 Å) and W^{6+} (0.62 Å) increases the unit cell volume from 128.05 $Å^3$ to 138.68 $Å^3$ which in turn causes the reflections shift towards lower angle side. In addition to this shifting, we observed splitting in X-ray reflections which is clearly seen in Fig. 1(a). In order to understand the splitting in the X-ray reflections, we have plotted the 2θ values of (-111) and (111) reflection as a function of composition and is shown in Fig. 1(b). We have given difference in 2θ values of these reflections in the same plot (i.e. Fig. 1(b)). This splitting may be due to any phase transition or changes in the lattice parameters with increasing the concentration of x in these compositions. Rietveld refinement was performed on all these compositions and observed to well fitted with P2/c space group and confirms the formation of all these compositions in monoclinic Wolframite structure. Refinement plots of all these compositions are shown in Fig. 2 (a-e) and the structural parameters such lattice parameter are given in Table 1(a) and Wyckoff positions and occupancies of x = 0.5 composition is given in Table 1(b). Fig. 3(a) and 3(b) show the variation of lattice parameters of $Ni_{1-x}(Zn_{1/2}Zr_{1/2})_x$ $W_{1-x}Nb_xO_4$ (x = 0.0 – 1.0) compositions. We have not observed much difference in lattice parameters (a, b and c) in spite of substitution of higher ionic radius elements in place of lower ionic radius elements whereas the monoclinic angle β shows an increment from 90.05°

to 91.73°. As $Ni_{1-x}(Zn_{1/2}Zr_{1/2})_xW_{1-x}Nb_xO_4$ (x = 0.0 – 1.0) compositions possess monoclinic Wolframite structure, splitting in X-ray reflections is explained with the variation in lattice parameters of these compositions. The d-spacing value of maximum intense (-111) and (111) reflections of all these compositions were calculated using the obtained lattice parameters from Rietveld refinement and the following formula and are given in Table 2.

$$\frac{1}{d^2_{(hkl)}} = \frac{1}{\sin^2\beta}\left[\frac{h^2}{a^2} + \frac{k^2\sin^2\theta}{b^2} + \frac{l^2}{c^2} - \frac{2hl\cos\beta}{ac}\right] \quad (2)$$

Where h, k and l represents the indices of the corresponding reflection whereas a, b, c and β represents the lattice parameters of respective compositions.

Fig. 3(c) shows the variation of $[d_{(-111)} - d_{(111)}]$ with increasing the concentration of x where the inset Figures indicate the variation of lattice parameters and splitting of maximum intense reflection with x concentration. It is clearly understood from this Fig. 3(c) that, increase in the lattice parameters enhances the difference in the d-spacing of (-111) and (111) reflections and is responsible for the splitting in X-ray reflections of all these compounds. Here, we have calculated d-spacing values for maximum intense reflections and the similar analysis can also be extended to explain the splitting of other reflections in higher angle side. In case of x = 0 composition, we have not seen splitting in maximum intense reflection in spite of very low value of $[d_{(-111)} - d_{(111)}]$ i.e. 0.0018 Å. This might be because of using higher scan step size (0.0169°) for all these measurements. We have not tried further by decreasing the scan step size because our instrument's minimum scan step size limit (0.004°) is higher than the required one. Hence, this splitting in the X-ray reflections of all these compositions in explained with lattice parameter variation.

Fig. 4 shows the crystal structure of $NiWO_4$ composition. Both the Ni^{2+} and W^{6+} are connected with six oxygen atoms forming distorted NiO_6 and WO_6 octahedra where the later one is more distorted in comparison with former one. B-site (W^{6+}) octahedra connect with other B-site (W^{6+}) octahedra by edge sharing and are extend along c-axis and form a zigzag chain type arrangement. A similar arrangement is observed in A-site (Ni^{2+}) octahedra also. In wolframite structure Ni^{2+} and W^{6+} occupy 2f and 2e Wyckoff positions respectively whereas the two distinguishable oxygen atoms occupy in the same site i.e. 4g. Oxygen O1 is connected to one B-site (W^{6+}) with one short terminal bond and two A-site (Ni^{2+}) cations relatively larger bonds. On the other hand oxygen O2 bridges two B-site (W^{6+}) cations and connected to one A-site (Ni^{2+}) cation. With substitution of higher ionic radius elements (Zn^{2+}, Zr^{4+} and Nb^{5+}) in place of lower ionic radius elements (Ni^{2+} and W^{6+}), the cation – oxygen bond lengths are elongated or compressed. In wolframite structure, B-site octahedra are distorted more and show an impact on the microwave dielectric properties of materials. Therefore, we have calculated B-site octahedral distortion of $Ni_{1-x}(Zn_{1/2}Zr_{1/2})_xW_{1-x}Nb_xO_4$ (x = 0.0 – 1.0) compositions using the obtained (Nb/W) – O bond length from Rietveld refinement and the following expression.[19] The calculated values are in the range of 10 to 20 % and are given in Table 4.

$$\text{Octahedral distortion, } \delta\ (\%) = \frac{(B-O\text{distance}_{\text{largest}}) - (B-O\text{distance}_{\text{smallest}})}{B-O\text{distance}_{\text{average}}} \quad (3)$$

Raman spectroscopy is an important and widely used experimental technique to understand the structural and vibrational properties of different class of materials. In general, the vibrational modes in ABO_4 compositions with Wolframite crystal structure are grouped into internal and external modes where the former modes are associated with $[(B_2O_8)^{4-}]_n$ polymeric anion in which the B-site cation is covalently bonded with oxygen atoms.[13] The

vibrational modes coming from A–O and lattice vibrational are grouped into external modes. Because of higher covalence nature of B – O bonds, internal vibrational modes are observed in higher frequency side whereas the external modes arising from A–O bonds will appear in lower frequency side. [25,26] Effect of substitution of different cations (Zn^{2+}, Zr^{4+}) at A-site and (Nb^{5+}) at B-sites of $NiWO_4$ compound was studied by collecting room temperature of Raman spectra of $Ni_{1-x}(Zn_{1/2}Zr_{1/2})_xW_{1-x}Nb_xO_4$ (x = 0.0 – 1.0) compositions and are shown in Fig. 5(a).

Group theoretical calculations predicted to have 36 vibrational modes for ABO_4 type compositions having Wolframite structure with P2/c space group and irreducible representation of all these modes is given below.[13]

$$\Gamma = 8A_g + 10B_g + 8A_u + 10B_u \quad (4)$$

Where, all the 'g' vibrations are Raman active whereas 'u' vibrations are IR active.

Fig. 5(a) show the Raman spectra of $Ni_{1-x}(Zn_{1/2}Zr_{1/2})_xW_{1-x}Nb_xO_4$ (x = 0.0 – 1.0) solid solution. In x = 0 compositions, we observe two Raman active modes in the high frequency range (1000 – 750 cm^{-1}) where the higher intensity mode at 893 cm^{-1} is assigned to the symmetric vibrations of short W – O bond as this frequency range is typical for symmetric vibrations of highly covalent bonds. Second mode at 776 cm^{-1} is assigned to the asymmetric vibrations of short W – O terminal bonds.[13] In the mid frequency range (750 – 500 cm^{-1}), four Raman modes were observed out of which two mode at 698.2 and 675.3 cm^{-1} are assigned to asymmetric stretching vibrations of W–O–W bridges whereas the rest lower frequency modes are assigned to symmetric stretching vibrations of W–O–W bridges. The modes corresponding to in-plane vibrations of short and longer W – O bonds are observed in 500 – 330 cm^{-1} frequency range whereas the strong mode at 368.1 cm^{-1} is assigned to the symmetric vibrations of NiO_6 octahedra. The reaming Raman active modes below 350 cm^{-1} are assigned to the out-of-plane vibrations of W – O bonds and lattice vibration in the wolframite crystal

structure.[13] The complete assignment of room temperature Raman spectra of $Ni_{1-x}(Zn_{1/2}Zr_{1/2})_xW_{1-x}Nb_xO_4$ (x = 0.0 – 1.0) compositions is shown in Fig. 5(a).

The Raman spectra of $Ni_{1-x}(Zn_{1/2}Zr_{1/2})_xW_{1-x}Nb_xO_4$ (x = 0.0 – 1.0) solid solution possess all the expected modes in accordance with Wolframite structure with P2/c space group. As the Raman modes are very sensitive to nature of bonding and distribution of cations at respective Wyckoff sites, Substitution of multiple cations (Zn^{2+}, Zr^{4+}) at Ni^{2+} site and Nb^{5+} in place of W^{6+} show considerable changes in the Raman spectra of these compositions. Change in the cation – oxygen bond lengths and masses of the constituent ions by substitution of multiple cations at A- and B-site of $NiWO_4$ might be responsible for the shift in the Raman modes of these compositions. The random distribution of (Zn^{2+}, Zr^{4+}) at Ni^{2+} site and Nb^{5+} at W^{6+} site is responsible for the change in the full width at half maxima (FWHM) and intensity of Raman active mode in all these compositions. Along with these changes, two more features were noticed in the Raman spectra of these compositions. One is the splitting in the symmetric stretching mode at 893 cm^{-1} and the other is, an additional mode is raised around 600 cm^{-1}. As the mode at 893 cm-1 is corresponding to the symmetric stretching vibrations of B–O bonds, splitting of this mode might be due to the electronegativity difference between Nb (1.6) and W (2.36) atoms present at the same site.[13] The lower electronegativity of Nb results in the formation of highly covalent bond with oxygen in comparison with W – O bond. In general, longer dimensional range associated with diffraction phenomena restricts us to predict the variation in the local bonding characteristics through powder X-ray diffraction measurements. Therefore, we have not observed any difference in the powder diffractograms of these compositions. On the other hand Raman spectroscopy is very sensitive to the distribution of cation at different sites which allow us to differentiate randomly distributed Nb^{5+} and W^{6+} ions in the present

$Ni_{1-x}(Zn_{1/2}Zr_{1/2})_xW_{1-x}Nb_xO_4$ (x = 0.0 – 1.0) solid solution. Raman spectra of all these compositions ($x \geq 0.25$) are deconvoluted and are shown in Fig. 5(b). It is clearly shown from these Figures that, the splitting in the strongest Raman mode (A_g mode ate 893 cm^{-1}) and the intensity of an additional mode around 600 cm^{-1} increase with increasing concentration of x. The proposed assignment of all the modes of $Ni_{1-x}(Zn_{1/2}Zr_{1/2})_xW_{1-x}Nb_xO_4$ (x = 0.0 – 1.0) compounds is given in Table 3.

In order to understand the chemical bonding characteristics of these compositions, we have done X-ray Photoelectron Spectroscopy (XPS) measurements on $Ni_{1-x}(Zn_{1/2}Zr_{1/2})_x$ $W_{1-x}Nb_xO_4$ (x = 0.0, 0.25, 0.50 and 0.75) compositions. Fig. 6a shows the high resolution XPS spectra of Ni (2p), W (4f) and O (1s) and binding energy of corresponding elements are given in Table 4. It is clear that in all these compositions (i.e. x = 0.0, 0.25, 0.50 and 0.75), Ni ($2p_{3/2}$) observed to has binding energy in the range 861.5 to 866.5 eV and is in good agreement with the literature[27, 28] for Ni^{2+} . On the other hand, W 4f level shows an asymmetric profile in the case of x = 0.0 and 0.25 compositions and is deconvoluted to two (i.e. $4f_{7/2}$ and $4f_{5/2}$). Whereas in the case of x = 0.50 and 0.75, these $4f_{7/2}$ and $4f_{5/2}$ are well separated and are in consistence with the earlier report[29] on materials having W^{6+}. This confirms that, in all $Ni_{1-x}(Zn_{1/2}Zr_{1/2})_xW_{1-x}Nb_xO_4$ (x = 0.0, 0.25, 0.5 and 0.75) compositions both Ni and W elements are in 2+ and 6+ oxidation states respectively. Fig. 6a indicates that the O (1s) level has an asymmetric shape which is deconvoluted into two. Out of these, the energy level in the range 533 – 535 eV is assigned to O (1s) level and the other level around 537 eV may be assign to the surface defect form in these compositions[30]. Binding energy values of O (1s) for all these compositions are given in Table 4. 2p core level spectra of Zn are shown in Fig. 6b. We can clearly see from this figure that there are two binding energy levels around 1026 eV and 1049 eV which are in consistence with the literature[31,32]. Lower

binding energy level at 1026 eV is assigned to core $2p_{3/2}$ level whereas another one is assigned to $2p_{1/2}$ and the binding energy values of these levels for all these compositions are given in Table 4. Boyuklimanli *et al.,* reported that the $3d_{5/2}$ core level of Zr was observed around 185.3 eV. Recently, a similar thing was reported by Dong *el al.,* [33,34]. In our present study on $Ni_{1-x}(Zn_{1/2}Zr_{1/2})_xW_{1-x}Nb_xO_4$ (x = 0.25, 0.5 and 0.75) compositions, we observed two spectral lines around 186 eV and 189 eV and these are assigned to 3d core levels of Zr element i.e. $3d_{5/2}$ and $3d_{3/2}$ respectively. In our present studies, we have observed a doublet around 211 eV. It was reported[35] that the $3d_{5/2}$ of Nb was observed around 208.2 eV. Hence, the spectral line observed at 211 eV is assigned to the $3d_{5/2}$ spectral line of Nb element present in all these compositions whereas the higher binding energy spectral line (i.e. 214 eV) is assigned to $3d_{3/2}$ of Nb. The binding energy values of spectral lines of the constituent elements of $Ni_{1-x}(Zn_{1/2}Zr_{1/2})_xW_{1-x}Nb_xO_4$ (x = 0.0, 0.25, 0.5 and 0.75) compositions are given in Table 4.

3.2 Density and Microstructural studies

Archimedes technique was used to measure the bulk densities of $Ni_{1-x}(Zn_{1/2}Zr_{1/2})_x W_{1-x}Nb_xO_4$ (x = 0.0 – 1.0) compositions with an accuracy of ± 0.005 and are given in Table 5 whereas the theoretical densities of all these compounds were calculated using the following formula.

$$\rho_{th} = \frac{nM}{NV}\ \text{g.cm}^{-3} \qquad (5)$$

Where, 'n' and 'M' gives the number of formula units per unit cell and molecular weight of the samples respectively whereas 'N' and 'V' represents the Avogadro's number (6.022×10^{23} mol^{-1}) and molar volume of the samples respectively. The molar volume (V_m) of all these compounds was calculated using the data obtained from Rietveld refinement.

Percentage of theoretical density of all these compounds was calculated using the measured (ρ_m) and calculated theoretical density (ρ_{th}) and the following formula. All the $Ni_{1-x}(Zn_{1/2}Zr_{1/2})_xW_{1-x}Nb_xO_4$ (x = 0.0 – 1.0) compounds posses more than 95% of theoretical density and are given in Table 5.

$$\rho(\%) = \frac{\rho_m}{\rho_{th}} \times 100 \quad (6)$$

FEI quanta 400 high resolution Scanning Electron Microscope was used to investigate the surface morphology of all these compositions. In order to get better micrographs, highly polished and thermally etched pellets were used for these measurements. Fig. 7(a – e) show the surface morphology of $Ni_{1-x}(Zn_{1/2}Zr_{1/2})_xW_{1-x}Nb_xO_4$ (x = 0.0 – 1.0) compositions and these micrographs reveal that, grain size observes to increase with increasing the concentration of x.

3. 3 Microwave dielectric characterization

Microwave dielectric properties such as dielectric constant, quality factor and temperature coefficient of resonant frequency of ceramic materials are influenced by extrinsic parameters such as secondary phases, porosity and density[36,37] which we can minimize by optimizing the processing conditions like calcination and sintering temperature of respective materials. On the other hand intrinsic parameters like ionic polarizability, molar volume, and structural characteristics of the materials also influence the microwave dielectric properties of ceramic materials.[38,39] In the present work, we have optimized the processing conditions like calcination temperature for obtaining single phase compositions with Wolframite structure and sintering temperature to achieve higher (≥ 95%) densification. Hence, we could succeed in minimizing the effect of extrinsic parameters on microwave dielectric properties of $Ni_{1-x}(Zn_{1/2}Zr_{1/2})_xW_{1-x}Nb_xO_4$ (x = 0.0 – 1.0) compositions. Therefore, in the present manuscript,

we report the effect of structural parameters on dielectric properties of these compositions with Wolframite structure.

3.3.1 Dielectric constant

Dielectric constant of $Ni_{1-x}(Zn_{1/2}Zr_{1/2})_xW_{1-x}Nb_xO_4$ (x = 0.0 – 1.0) compounds was measured using Hakki – Colemann method and are given in Table 5. Fig. 8 shows the variation of dielectric constant of $Ni_{1-x}(Zn_{1/2}Zr_{1/2})_xW_{1-x}Nb_xO_4$ (x = 0.0 – 1.0) compositions from which we can indicate that, dielectric constant observed to increase with increasing the concentration of x. In general, dielectric constant of ceramic materials depend extrinsic parameters such as density, porosity and secondary phases[40] present in compounds. In the present study, as all these compounds possess more than 95% theoretical density with less porosity and show single phase with Wolframite crystal structure, the variation in the dielectric constant is explained with intrinsic parameter such as polarizability. Substitution of higher polarizable Zn^{2+} (2.04 Å^3), Zr^{4+} (3.25 Å^3) ions at Ni^{2+} (1.23 Å^3) site and Nb^{5+} (3.97 Å^3) in place of W^{6+} (3.20 Å^3) increases the polarizability of the compounds[17] which in turn increases the dielectric constant of these compounds. The polarizability of $Ni_{1-x}(Zn_{1/2}Zr_{1/2})_x W_{1-x}Nb_xO_4$ (x = 0.0 – 1.0) compounds is calculated using Shannon additive rule[17] and are given in Table 5.

$$\alpha_D(Ni_{1-x}(Zn_{1/2}Zr_{1/2})_xW_{1-x}Nb_xO_4) = (1-x)\alpha_D(Ni^{2+}) + 0.5x\alpha_D(Zn^{2+} + Zr^{4+}) + (1-x)\,\alpha_D(W^{6+}) + x\alpha_D(Nb^{5+}) + 4\alpha_D(O^{2-}) \quad (7)$$

3.3.2 Quality factor

Reflection cavity technique was used to measure the quality factor ($Q\times f$) of $Ni_{1-x}(Zn_{1/2}Zr_{1/2})_xW_{1-x}Nb_xO_4$ (x = 0.0 – 1.0) compounds and are given in Table 5. Fig. 9 shows the variation of quality factor of $Ni_{1-x}(Zn_{1/2}Zr_{1/2})_xW_{1-x}Nb_xO_4$ (x = 0.0 – 1.0) compositions and

reveal that with increasing the concentration of *x* from 0.0 to 1.0, the quality factor gradually increases from 23500 GHz to 53450 GHz. It was reported that the quality factor of ceramic materials depend on porosity, density and secondary phases[16,40] present in the materials which can minimize through optimization of processing conditions. Along with structural parameters such as bonding characteristics and packing fraction[14], nature of elements that are accommodated in the crystal structure[41] can also influence the quality factor of ceramic materials. Pullar *et al.* observed that the quality factor of AWO_4 (A: Mg, Zn, Ni and Co) compounds with wolframite structure depend on the extrinsic parameters such as density and microstructure of these compounds and concluded that, in-homogeneous and discontinues grain growth was responsible for the lower quality factor of $MgWO_4$.[16] On the other hand, Choi *et al.* reported $AMoO_4$ (A: Mg, Zn and Mn) compounds with Wolframite structure in which all these compounds posses more than 95% theoretical density and explained the variation in quality factor of these compounds with ionic radius of A-site cation.[18] Correlation among sintering temperature, quality factor and atomic packing fraction was reported by Liao *et al.* in $ZnTiNbTaO_8$ compound where they showed that the compound with higher packing factor posses higher quality factor.[42]

In addition to these structural parameters, presence of localized 3d electron in the constituent ions induces conductivity which in turn influence the quality factor of the compounds.[41] In this view, researchers investigated the correlation among the quality factor and localized 3d electrons present in the constituent ions in compounds with Perovskite and Columbite crystal structure.[41,43] The variation in quality factor of $A^{2+}TiO_3$ (A: Ni, Mg and Mn) compounds was explained with the presence of localized 3d electrons in divalent metal ions and conclude that, presence of localized 3d electrons in Ni^{2+} ($3d^8$) and Mn^{2+} ($3d^5$) were responsible for their lower quality factor in comparison with Mg^{2+} ($3d^0$) substituted compound.[43] In a similar way, Lee *et al.* correlated the variation in quality factor of MNb_2O_6

(M: Ca, Mn, Co and Zn) compounds with Columbite structure with the localized 3d electron present in the ions.[41] Recently, Kim *et al.* reported the microwave dielectric properties of ABO_4 (A: Ni, Mg, Zn and B: W, Mo) compounds with Wolframite crystal structure where they observed an interesting correlation among atomic packing fraction and quality factor of all these compounds except in $NiWO_4$ and explained its lower quality factor with localized 3d electrons which induce conductivity in $NiWO_4$.[20]

In the present studies on $Ni_{1-x}(Zn_{1/2}Zr_{1/2})_xW_{1-x}Nb_xO_4$ (x = 0.0 – 1.0) compounds, as we mentioned in the powder X-ray diffraction analysis that the unit cell volume increase with increasing the concentration of x which in turn decrease the packing fraction of these compounds according to equation (8) given below.[14] We have calculated the packing fraction of all these compounds and are given in Table 4. With increasing the concentration of x, we observed an enhancement in quality factor of $Ni_{1-x}(Zn_{1/2}Zr_{1/2})_xW_{1-x}Nb_xO_4$ (x = 0.0 – 1.0) compositions in spite their lower packing factor values which is clearly shown in Fig. 9. This contradictory behaviour in quality factor of these compositions is explained with localized 3d electrons present in the constituent ions. When we are moving from Ni^{2+} rich compounds to Ni^{2+} poor compounds, the conductivity of the compounds will decrease because of replacement of divalent metal Ni^{2+} ($3d^8$) having localized 3d electrons with empty Zr^{4+} ($4d^0$) and completely filled Zn^{2+} ($3d^{10}$) ions at A-site of these compounds and is confirmed by measuring the AC conductivity of all these compositions using an expression (9) given below.

$$\text{Packing fraction (\%)} = \frac{\text{Volume of packed ions}}{\text{Volume of primitive unitcell}} = \frac{\text{Volume of packed ions}}{\text{Volume of unitcell}} \times Z = \frac{4\pi/3 \times (r_A^3 + r_B^3 + 4 \times r_O^3)}{\text{Volume of unitcell}} \times Z \quad (8)$$

Where, r_A, r_B and r_o represents ionic radius of A, B-site cations and O^{2-} respectively. Z is the number formula units per unit cell.

AC conductivity, $\sigma_{ac} = \varepsilon' \varepsilon_0 \omega \tan\delta$ (9)

Where, ε' and ε_0 represents the real part and free space permittivity respectively whereas ω and $\tan\delta$ gives the angular frequency and loss tangent of the compositions.

From expression, we can clearly indicate that, the conductivity is directly proportional to the loss tangent. The measured AC conductivity values of these compositions is shown in insight of Fig. 9 and from this we can see the decrease in AC conductivity of these compositions with increasing the concentration of x which in turn decreases the losses present in the compositions and hence, the composition with lower Ni^{2+} concentration possess higher quality factor. Therefore, enhancement in the quality factor of $Ni_{1-x}(Zn_{1/2}Zr_{1/2})_xW_{1-x}Nb_xO_4$ (x = 0.0 – 1.0) compositions is explained with d electrons present in the constituent ions of these compositions and the variation quality factor of these compounds is shown in Fig. 9.

3.3.3 Temperature coefficient of resonant frequency (τ_f)

Temperature coefficient of resonant frequency (τ_f) is key parameter of any dielectric resonator materials which decides the performance of these dielectric resonators at different atmospheric conditions and is related to temperature coefficient of dielectric constant (τ_ε) by the following relation

$$\tau_f = -\alpha - \frac{1}{2}\tau_\varepsilon \quad (10)$$

Where α represents the coefficient of thermal expansion of these resonators and in general it is in the range of 10 ppm/^{o}C for all the ceramic materials. As α is very low, the variation of τ_f predominantly depends on temperature coefficient of dielectric constant (τ_ε).

From Clausius – Mosotti equation one can obtain the temperature coefficient of dielectric constant (τ_ε) and is given below[44]

$$\tau_\varepsilon = \frac{1}{\varepsilon}\left(\frac{\partial \varepsilon}{\partial T}\right) = \frac{(\varepsilon - 1)(\varepsilon + 2)}{\varepsilon}(A + B + C) \qquad (11)$$

$$A = -\frac{1}{3V}\left(\frac{\partial V}{\partial T}\right)_P \qquad B = \frac{1}{3\alpha_m}\left(\frac{\partial \alpha_m}{\partial V}\right)_T \left(\frac{\partial V}{\partial T}\right)_P \qquad C = \frac{1}{3\alpha_m}\left(\frac{\partial \alpha_m}{\partial T}\right)_V$$

Where, 'α_m' and 'V' represents the polarizability and volume of macroscopic, small sphere respectively.

According to Bosman and Havinga,[44] the first two terms A and B are related with the volume expansion with increasing the temperature which are having nearly equal magnitude and opposite sign, therefore the effect of A and B on τ_ε is negligible. The third term C gives the restoring force acting on the ions and this restoring force depends on the shape of the potential well, hence the term C is explained with the structural parameters such as octahedral distortions in the compounds.

An invar cavity attached to programmable hot plate was used to measure the temperature coefficient of resonant of frequency (τ_f) of $Ni_{1-x}(Zn_{1/2}Zr_{1/2})_xW_{1-x}Nb_xO_4$ (x = 0.0 – 1.0) compositions and are given in Table 5. Fig. 10 shows the variation of τ_f of $Ni_{1-x}(Zn_{1/2}Zr_{1/2})_xW_{1-x}Nb_xO_4$ (x = 0.0 – 1.0) compositions and from this we can indicated that, with increasing concentration of x, the τ_f values varied from -26 ppm/^{o}C to -49 ppm/^{o}C. As the temperature coefficient of resonant frequency depends on the structural characteristics of materials, Kim *et al.* reported[19] the variation of τ_f with the average octahedral distortion in $ATiO_3$, ATa_2O_6 and AWO_4 (A: Ni, Mg and Co) compositions. With increasing the octahedral distortion, the restoring forces between the cation and oxygen will increase which indirectly

influence the temperature coefficient of resonant frequency of these compounds.[19] A similar analysis was reported by Kim *et al.* in $(Zn_{1/3}B_{2/3}^{5+})_xTi_{1-x}O_2$ with (B: Nb, Ta) Rutile structure [45]where the deviation of τ_f from zero is explained with the increase in the octahedral distortion of compounds. In $Ni_{1-x}(Zn_{1/2}Zr_{1/2})_xW_{1-x}Nb_xO_4$ compounds, substitution of higher ionic radius[22] elements Zn^{2+} (0.74 Å), Zr^{4+} (0.72 Å) and Nb^{5+} (0.69 Å) influence the cation – oxygen bond lengths and resulting the increase in the $(Nb/W)O_6$ octahedral distortion from 10 % to 20 % which in turn deviate τ_f away from zero i.e. -26 ppm/^{o}C to -49 ppm/^{o}C. Hence, the variation in τ_f of $Ni_{1-x}(Zn_{1/2}Zr_{1/2})_xW_{1-x}Nb_xO_4$ (x = 0.0 – 1.0) compositions is explained with B-site octahedral distortion and is shown in Fig. 10.

Conclusions

We have successfully synthesized $Ni_{1-x}(Zn_{1/2}Zr_{1/2})_xW_{1-x}Nb_xO_4$ (x = 0.0 – 1.0) compositions via conventional solid state reaction method and observed to possess monoclinic Wolframite crystal structure with P2/c space group. The splitting in the powder X-ray diffractograms of these compounds is explained with the lattice parameter by calculating d-spacing value of (-111) and (111) reflection of these compounds. The additional modes raised in Zn^{2+}, Zr^{4+} and Nb^{5+} substituted compositions are explained with the electronegativity difference between the cations (Nb and W) at B-site of these compositions whereas the variation in the FWHM and intensity of Raman modes is attributed to the presence of randomly distributed multiple cations (Ni^{2+}, Zn^{2+} and Zr^{4+} at A-site and Nb^{5+}, W^{6+} in B-site) at a particular site. XPS analysis reveals that all the elements are in their respective oxidation state in these compositions. Increase in grain size was observed when we are moving from Ni^{2+} rich compositions to Ni^{2+} poor composition which is clearly seen from the Scanning Electron Micrographs of these compositions. All these compositions posses more than 95% theoretical density with good microwave dielectric properties (ε_r ~ 12 – 15, $Q\times f$ ~ 23500 –

53000 GHz and τ_f ~ -25 ppm/^{o}C to -49 ppm/^{o}C). The enhancement in dielectric constant and quality factor of these compositions is correlated with polarizability and 3d electrons present in constituent ions of respective compositions. The variation in τ_f is explained with the increase in the B-site octahedral distortion in these compositions.

Acknowledgements

The authors are thankful to University Grant Commission, New Delhi, India for providing financial assessment in the form of Senior Research Fellowship. Author specially thanks Prof. S. Ramaprabhu and Prof. B. Viswanathan for allowing me to use X-ray photo electron spectroscopy instrument. Author thanks Ashok P, Department of Physics, IIT Madras for his cooperation in doing XPS measurements.

References

(1) R. J. Cava, *J. Mater. Chem.*, 2001, **11**, 54.

(2) I.M. Reaney, and D. Iddles, *J. Am. Ceram. Soc.* 2006, **89**, 2063.

(3) M.T. Sebastian, Elsevier publishing group, 2008.

(4) H. Zheng, G. D. C. de Fyorgyfalva, and I.M. Raney, *J. Mater. Sci*. 2005, **40**, 5207.

(5) C. –F. Tseng, C. –L. Huang, N. –R. Yang, and C. –H. Hsu, *J. Am. Ceram. Soc.* 2006, **89**, 465.

(6) H. Yamada, T. Okawa, Y. Yohdo, and H. Ohsato, *J. Eur. Ceram. Soc.* 2006, **26**, 2059.

(7) H. –J. Lee, I. –T. Kim, and K.S. Hong, *Jpn. J. Appl. Phys.* 1997, **36**, L1318.

(8) G.-K. Choi, S.-Y. Cho, J.-S. An, and K. S. Hong, *J. Eur. Ceram. Soc.* 2006, **26**, 2011.

(9) G.-K. Choi, J.-R. Kim, S. H. Yoon and K. S. Hong, *J. Eur. Ceram. Soc.* 2007, **27**, 3063.

(10) E. S. Kim, S.-H. Kim, and B. I. Lee, *J. Eur. Ceram. Soc.* 2006, **26**, 2101.

(11) D. Zhou, W.-B. Li, L.-X. Pang, J. Guo, Z.-M. Qi, T. Shao, X. Yao and C. A. Randall, *Dalton Trans.* 2014, **43**, 7290.

(12) D. Zhou, L.-X. Pang, J. Guo, Z.-M. Qi, T. Shao, X. Yao and C. A. Randall, *J. Mater. Chem.* 2012, **22**, 21412.

(13) M. Daturi, G. Busca, M. M. Borel, A. Leclaire, and P. Piaggio, *J. Phys. Chem. B* 1997, **101**, 4358.

(14) E. S. Kim, B. S. Chun, R. Freer and R. J. Cernik, *J. Eur. Ceram. Soc.* 2010, **30**, 1731.

(15) S. H. Yoon, D. W. Kim, S. Y. Cho and K. S. Hong, *J. Eur. Ceram. Soc.* 2006, **26**, 2051.

(16) R. C. Pullar, S. Farrah and N. M. Alford, *J. Eur. Ceram. Soc.* 2007, **27**, 1059.

(17) R. D. Shannon, *J. Appl. Phys.* 1993, **73**, 348.

(18) G. K. Choi, J. R. Kim, S. H. Yoon, and K. S. Hong, *J. Eur. Ceram. Soc.* 2007, **27**, 3063.

(19) E. S. Kim and C. J. Jeon, *Applications of Ferroelectrics, 2009. ISAF 2009.* 2009, 1.

(20) E. S. Kim, C. J. Jeon, and P. G. Clem, *J. Am. Ceram. Soc.* 2012, **95**, 2934.

(21) A. C. Larson, and R. B. von Dreele, General Structural Analysis System (GSAS), Los Alamos National Laboratories, Los Alamos, NM, 1990.

(22) B. H. Toby, *J. Appl. Crystallogr.* 2001, **34**, 210.

(23) B. W. Hakki and P. D. Coleman, *IRE Trans. Microwave. Theory. Tech.* 1960, **8**, 402.

(24) R. D. Shannon, *Acta. Cryst. A* 1976, **32**, 751.

(25) A. S. Barker, Jr. *Phy. Rev.* 1964, **135**, A742.

(26) S. P. S. Porto and J. F. Scott, *Phy. Rev.* 1967, **157**, 716.

(27) M. G. Thube, S. K. Kulkarni, D. Huerta, and A. S. Nigavekar, *Phys. Rev. B* **34**, 6874.

(28) A. Maione and M. Devillers, *J. Solid. State. Chem.* 2004, **177**, 2339.

(29) G. P. Halada and C. R. Clayton, *J. Vac. Sci. Technol. A*, 1993, **11**, 2342.

(30) M. N. Mancheva, R. S. Iordanova, D. G. Klissurski, G. T. Tyuliev and B. N. Kunev, *J. Phys. Chem. C* 2007, **111**, 1101.

(31) R. D. Seals, R. Alexander, L. T. Taylor and J. G. Dillard, *Inorg. Chem.* 1973, **12**, 2485.

(32) L. G. Mar, P. Y. Timbrell and R. N. Lamb, *Thin Solid Films* 1993, **223**, 341.

(33) T. H. Boyuklimanli and J. H. Simmons, *J. Non-cryst. Solids* 1989, **120**, 262.

(34) K. F. Dong, H. H. Li, Y. G. Peng, G. Ju, G. M. Chow and J. S. Chen, *Sci. Rep.* 2014, 4.

(35) D. D. Sarma and C. N. R. Rao, *J. Electron Spectrosc. Relat. Phenom.* 1980, **20**, 25.

(36) M. H. Liang, C. T. Hu, H. F. Cheng, I. N. Lin, and J. Steeds, *J. Eur. Ceram. Soc.* 2001, **21**, 2759.

(37) W. S. Kim, E. S. Kim and K. H. Yoon, *J. Am. Ceram. Soc.* 1999, **82**, 2111.

(38) S. R. Kiran, G. Sreenivasulu, V. R. K. Murthy, V. Subramanian, and B. S. Murthy, *J. Am. Ceram. Soc.* 2012, **95**, 1973.

(39) X. C. Fan, X. M. Chen and X. Q. Liu, *Chem. Mater.* 2008, **20**, 4092.

(40) N. Ichinose and T. Shimada, *J. Eur. Ceram. Soc.* 2006, **26**, 1755.

(41) H. –J. Lee, K. –S. Hong and S. –J. Kim, *Mater. Res. Bull.* 1997, **32**, 847.

(42) Q. Liao, L. Li, X. Ren and X. Ding, *J. Am. Ceram. Soc.* 2011, **94**, 3237.

(43) J. –H. Sohn, Y. Inaguma, S. –O. Yoon, M. Itoh, T. Nakamura, S. –J. Yoon and H. –J. Kim, *Jpn. J. Appl. Phys.* 1994, **33**, 5466.

(44) A. J. Bosman and E. E. Havinga, *Phys. Rev.* 1963, **129**, 1593.

(45) E.S. Kim and D. H. Kang, *Ceram. Int.* 2008, **34**, 883.

Table captions

Table 1(a). Lattice parameter (a, b, c and β) of $Ni_{1-x}(Zn_{1/2}Zr_{1/2})_xW_{1-x}Nb_xO_4$ compositions.

Table 1(b). Wyckoff positions and occupancies of $x = 0.5$ composition.

Table 2. Calculated d-spacing values of $Ni_{1-x}(Zn_{1/2}Zr_{1/2})_xW_{1-x}Nb_xO_4$ compositions.

Table 3. Proposed Raman mode assignment in $Ni_{1-x}(Zn_{1/2}Zr_{1/2})_xW_{1-x}Nb_xO_4$compositions with Wolframite structure.

Table 4. Binding energies of constituent element of $Ni_{1-x}(Zn_{1/2}Zr_{1/2})_xW_{1-x}Nb_xO_4$ ($x = 0.0$, 0.25, 0.50 and 0.75) compositions

Table 5. Density (ρ), polarizability (α_D), dielectric constant (ε_r), quality factor ($Q \times f$), temperature coefficient resonant frequency (τ_f), packing fraction (P.F) and B-site octahedral distortion of $Ni_{1-x}(Zn_{1/2}Zr_{1/2})_xW_{1-x}Nb_xO_4$ compositions.

Figure captions

Fig. 1(a). Powder X-ray diffractions patterns of $Ni_{1-x}(Zn_{1/2}Zr_{1/2})_xW_{1-x}Nb_xO_4$compositions.

Fig. 1(b). Variation of 2θ values of (-111) and (111) reflections and their difference with concentration of *x*.

Fig. 2. Rietveld refinement plot of (a) x = 0.0 (b) x = 0.25 (c) x = 0.50 (d) x = 0.75 (e) x = 1.0 compositions. (Observed powder X-ray diffraction data (o), calculated diffraction pattern with red solid line and difference plot with Magenta color).

Fig. 3(a). Lattice parameters (*a*, *b* and *c*) of $Ni_{1-x}(Zn_{1/2}Zr_{1/2})_xW_{1-x}Nb_xO_4$compositions.

Fig. 3(b). Monoclinic angle (β) of $Ni_{1-x}(Zn_{1/2}Zr_{1/2})_xW_{1-x}Nb_xO_4$compositions.

Fig. 3(c). Variation of $d_{(-111)} - d_{(111)}$ in $Ni_{1-x}(Zn_{1/2}Zr_{1/2})_xW_{1-x}Nb_xO_4$solid solution. (Inset shows the lattice parameter variation and splitting of maximum intense reflection)

Fig. 4. Crystal structure of $NiWO_4$ composition.

Fig. 5(a). Raman spectra of $Ni_{1-x}(Zn_{1/2}Zr_{1/2})_xW_{1-x}Nb_xO_4$compositions.

Fig. 5(b). Deconvoluted Raman spectra of $Ni_{1-x}(Zn_{1/2}Zr_{1/2})_xW_{1-x}Nb_xO_4$compositions.

Fig. 6a. High-resolution XPS spectra of (i) Ni (2p), (ii) W (4f) and (iii) O (1s) core levels in $Ni_{1-x}(Zn_{1/2}Zr_{1/2})_xW_{1-x}Nb_xO_4$ compositions.

Fig. 6b. High-resolution XPS spectra of (i) Zn (2p), (ii) Zr (3d) and (iii) Nb (3d) core levels in $Ni_{1-x}(Zn_{1/2}Zr_{1/2})_xW_{1-x}Nb_xO_4$ compositions.

Fig. 7. Scanning electron micrograph of $Ni_{1-x}(Zn_{1/2}Zr_{1/2})_xW_{1-x}Nb_xO_4$compositions (a) x = 0.0 sintered at 1200 ^oC (b) x = 0.25 sintered at 1250 ^oC (c) x = 0.50 sintered at 1275 ^oC (d) x = 0.75 sintered at 1275 ^oC (e) x = 1.0 sintered at 1300 ^oC.

Fig. 8. Variation of dielectric constant and ionic polarizability of $Ni_{1-x}(Zn_{1/2}Zr_{1/2})_xW_{1-x}Nb_xO_4$ compositions.

Fig. 9. Variation of quality factor of $Ni_{1-x}(Zn_{1/2}Zr_{1/2})_xW_{1-x}Nb_xO_4$ compositions. (Insets show the variation in (i) AC conductivity and (ii) packing fraction of these compositions with increasing concentration of x)

Fig. 10. Correlation among B-site octahedral distortion and temperature coefficient of resonant frequency of $Ni_{1-x}(Zn_{1/2}Zr_{1/2})_xW_{1-x}Nb_xO_4$compositions.

Table 1(a). Lattice parameter (a, b, c and β) of $Ni_{1-x}(Zn_{1/2}Zr_{1/2})_xW_{1-x}Nb_xO_4$ compositions.

x	a (Å)	b (Å)	c (Å)	$\beta°$
0.0	4.600	5.666	4.912	90.05
0.25	4.655	5.664	4.963	90.49
0.5	4.714	5.662	5.01	90.94
0.75	4.766	5.665	5.048	91.23
1.0	4.805	5.673	5.082	91.71

Table 1(b). Wyckoff positions and occupancies of x = 0.5 composition.

Atom	x	y	z	Occupancy
Ni	0.5	0.678(4)	0.25	0.50
Zn	0.5	0.678(4)	0.25	0.25
Zr	0.5	0.678(4)	0.25	0.25
W	0	0.177(2)	0.25	0.50
Nb	0	0.177(2)	0.25	0.50
O1	0.226(1)	0.126(8)	0.917(2)	1.0
O2	0.272(2)	0.379(3)	0.383(2)	1.0

Table 2. Calculated d-spacing values of $Ni_{1-x}(Zn_{1/2}Zr_{1/2})_xW_{1-x}Nb_xO_4$ compositions.

x	$d_{(-111)}$ (Å)	$d_{(111)}$ (Å)	$d_{(-111)} - d_{(111)}$ (Å)
0.0	2.88836	2.88651	0.00185
0.25	2.92023	2.90195	0.01828
0.50	2.95232	2.91717	0.03515
0.75	2.97845	2.93235	0.04610
1.0	3.00667	2.94157	0.06510

Table 3. Proposed Raman mode assignment in $Ni_{1-x}(Zn_{1/2}Zr_{1/2})_xW_{1-x}Nb_xO_4$ compositions with Wolframite structure.

Symmetry	$x = 0.0$	$x = 0.25$	$x = 0.50$	$x = 0.75$	$x = 1.0$
$\mathbf{A_g}$	893.0	895.9 (878.9)	896.5 (873.5)	896.8 (859.5)	881.6 (853.2)
$\mathbf{B_g}$	776.0	776.2	767.4	758.1	756.9
$\mathbf{A_g}$	698.2	696.9	694.7	678.9	674.9
$\mathbf{B_g}$	675.3	666.1	657.7	645.4	640.9
-	-	615.3	598.4	580.0	585.7
$\mathbf{A_g}$	552.7	543.1	534.2	525.8	517.1
$\mathbf{B_g}$	515.2	507.2	483.8	473.7	474.0
$\mathbf{A_g}$	421.3	412.5	410.6	408.7	413.2
$\mathbf{B_g}$	383.5	379.9	357.7	356.6	367.5
$\mathbf{A_g}$	368.1	360.6	315.2	310.7	340.8
$\mathbf{B_g}$	330.4	322.6	292.5	288.8	311.0
$\mathbf{A_g}$	311.0	298.9	286.1	279.7	284.8
$\mathbf{B_g}$	291.0	263.0	247.3	246.2	249.3
$\mathbf{A_g}$	227.2	226.5	221.1	204.2	205.8
$\mathbf{B_g}$	214.4	203.3	194.6	184.7	190.9
$\mathbf{B_g}$	202.5	170.6	161.9	155.8	155.3
$\mathbf{B_g}$	179.7	148.6	142.0	130.6	142.4
$\mathbf{A_g}$	153.3	133.9	126.9	117.9	129.9
$\mathbf{B_g}$	101.8	101.1	101.5	96.0	124.3

Table 4. Binding energies of constituent element of $Ni_{1-x}(Zn_{1/2}Zr_{1/2})_xW_{1-x}Nb_xO_4$ (x = 0.0, 0.25, 0.50 and 0.75) compositions

Element	Spectral line	x = 0.0	x = 0.25	x = 0.50	x = 0.75
Ni	**$2p_{3/2}$**	861.2 (±0.15)	861.5 (±0.23)	862.4 (±0.04)	866.5 (±0.15)
W	**$4f_{7/2}$**	39.7 (±0.09)	39.4 (±0.13)	39.9 (±0.12)	39.8 (±0.14)
	$4f_{5/2}$	43.2 (±0.06)	42.9 (±0.15)	42.2 (±0.15)	41.9 (±0.12)
O	**1s**	533.5 (±0.07)	533.8 (±0.05)	534.8 (±0.06)	534.6 (±0.04)
Zn	**$2p_{3/2}$**	-	1026.2 (±0.07)	1026.4 (±0.03)	1026.1 (±0.08)
	$2p_{1/2}$	-	1049.2 (±0.04)	1049.6 (±0.09)	1049.3 (±0.03)
Zr	**$3d_{5/2}$**	-	187.2 (±0.09)	186.8 (±0.08)	186.6 (±0.05)
	$3d_{3/2}$	-	189.6 (±0.05)	189.1 (±0.04)	188.9 (±0.03)
Nb	**$3d_{5/2}$**	-	213.2 (±0.08)	211.3 (±0.06)	211.4 (±0.07)
	$3d_{3/2}$	-	215.3 (±0.03)	214.0 (±0.07)	214.1 (±0.08)

Table 5. Density (ρ), polarizability (α_D), dielectric constant (ε_r), quality factor ($Q\times f$), temperature coefficient resonant frequency (τ_f), packing fraction (P.F) and B-site octahedral distortion of $Ni_{1-x}(Zn_{1/2}Zr_{1/2})_xW_{1-x}Nb_xO_4$ compositions.

x	ρ (%)	α_D (Å^3)	ε_r	$Q\times f$ (GHz)	τ_f (ppm/°C)	P.F (%)	δ (%)
0.0	95.2	12.470	12.4	23400	-26.2	69.50	10.3
0.25	96.1	13.016	13.2	28700	-29.1	68.29	15.6
0.50	96.7	13.562	14.8	32650	-34.8	67.07	17.3
0.75	97.2	14.109	15.2	41250	-44.7	65.86	18.7
1.0	97.8	14.655	16.2	53350	-49.2	64.63	20.11

Fig. 1(a). Powder X-ray diffractions patterns of $Ni_{1-x}(Zn_{1/2}Zr_{1/2})_xW_{1-x}Nb_xO_4$ compositions.

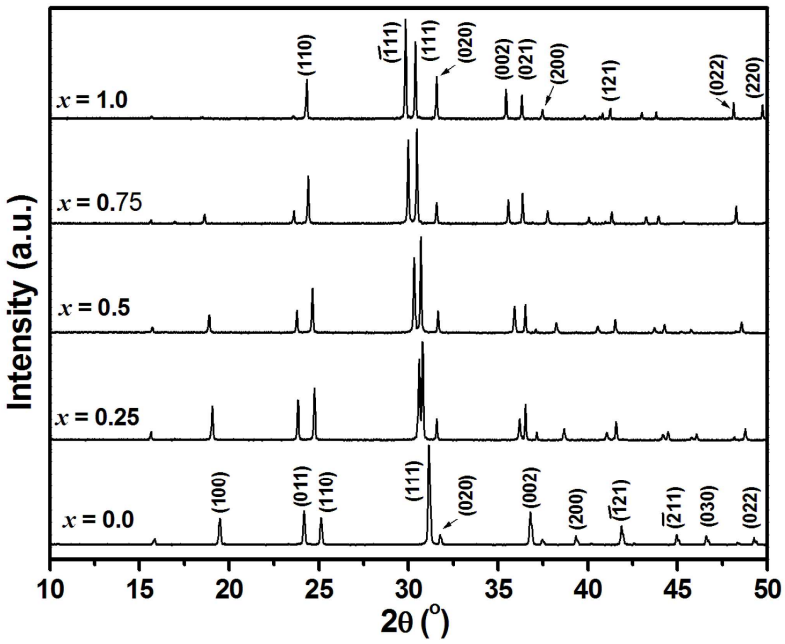

Fig. 1(b). Variation of 2θ values of (-111) and (111) reflections and their difference with concentration of *x*.

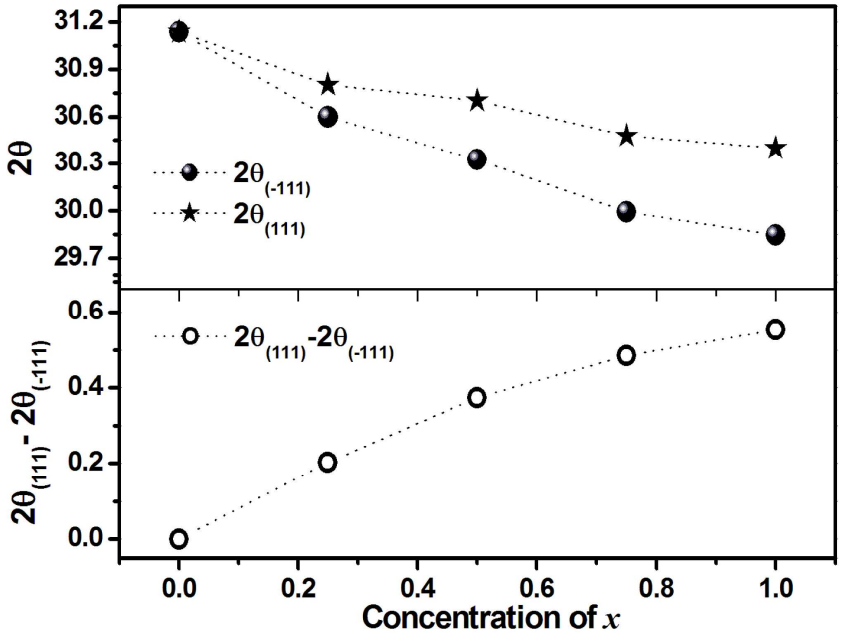

Fig. 2. Rietveld refinement plot of (a) x = 0.0 (b) x = 0.25 (c) x = 0.50 (d) x = 0.75 (e) x = 1.0 compositions. (Observed powder X-ray diffraction data (o), calculated diffraction pattern with red solid line and difference plot with Magenta color).

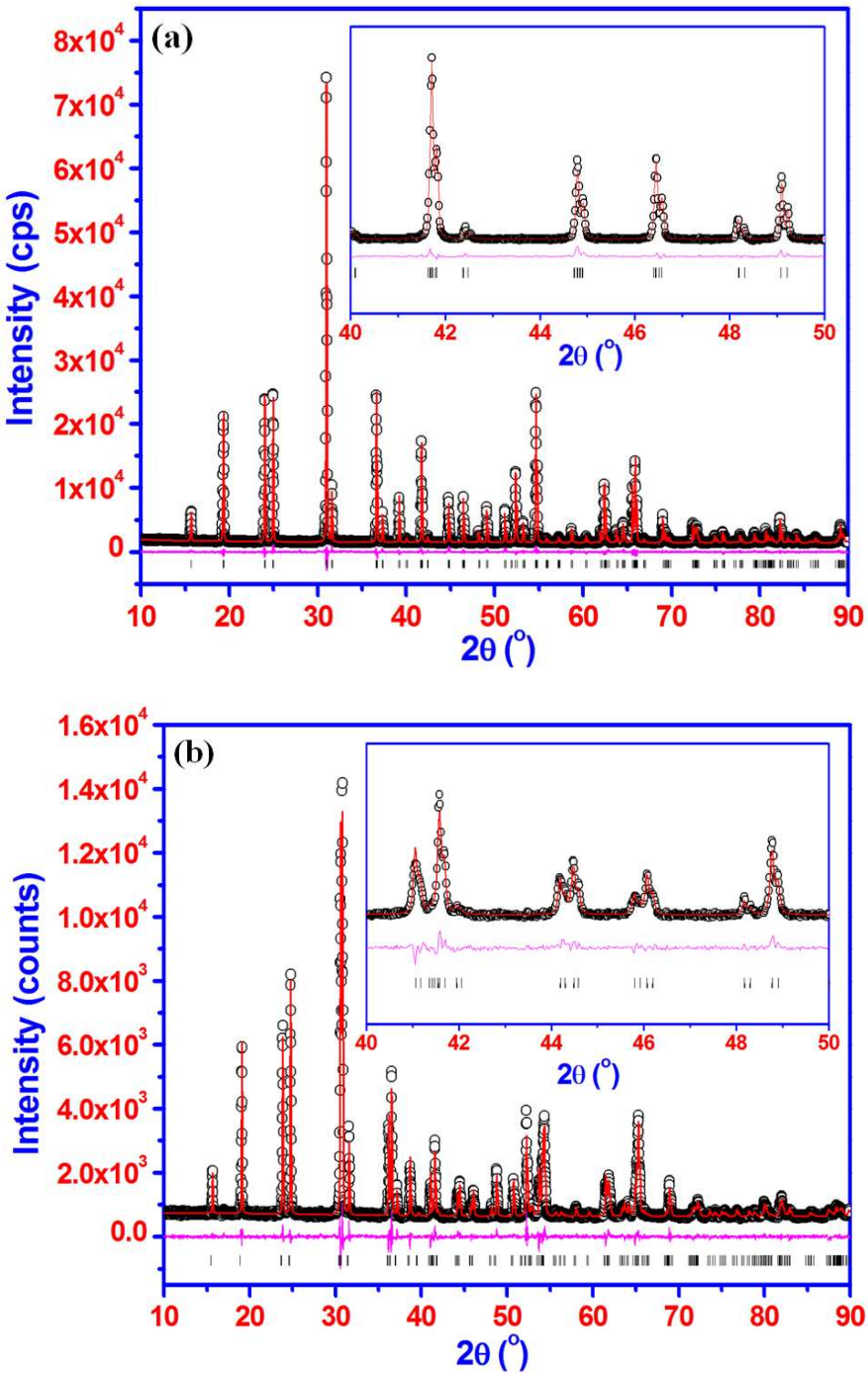

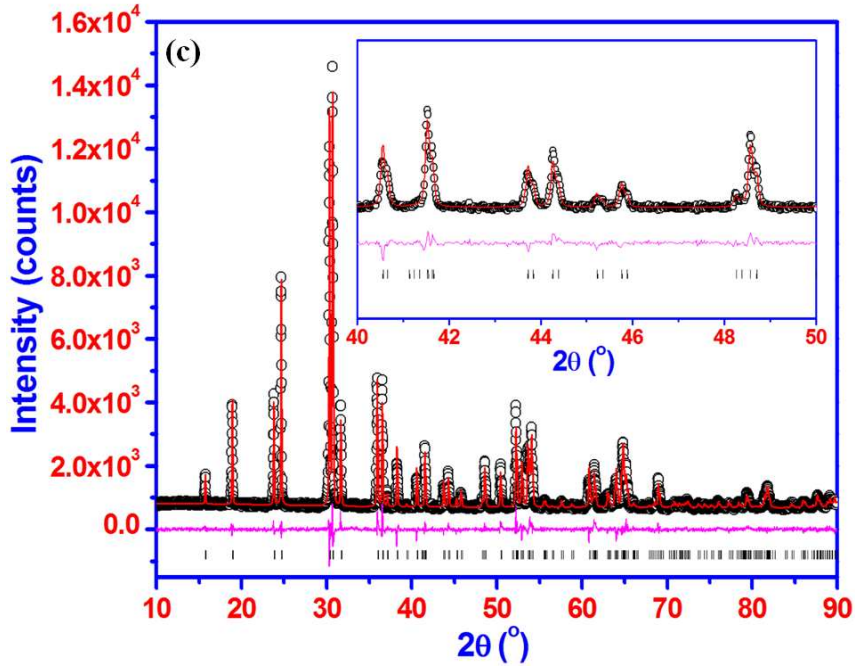

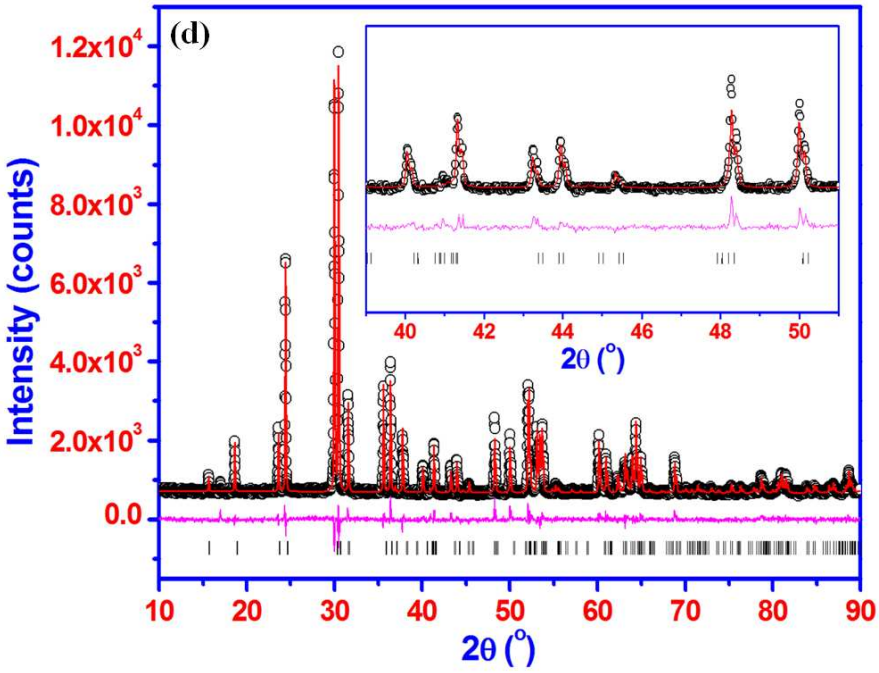

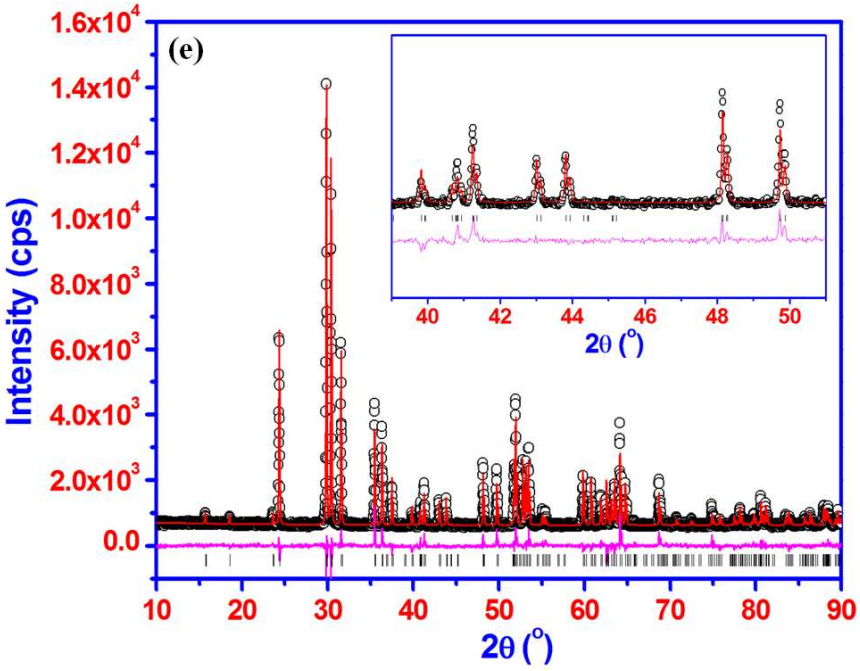

Fig. 3(a). Lattice parameters (*a*, *b* and *c*) of $Ni_{1-x}(Zn_{1/2}Zr_{1/2})_xW_{1-x}Nb_xO_4$ compositions.

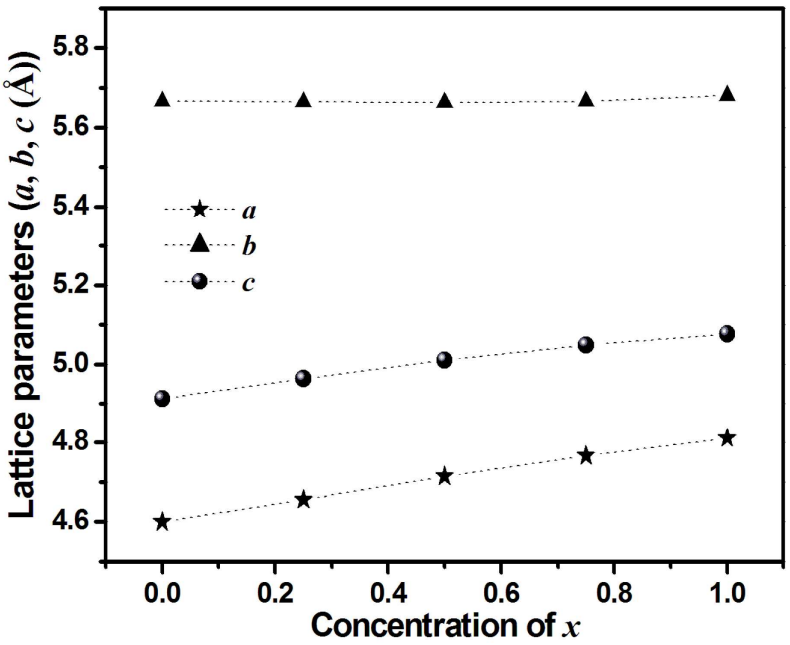

Fig. 3(b). Monoclinic angle (β) of $Ni_{1-x}(Zn_{1/2}Zr_{1/2})_xW_{1-x}Nb_xO_4$ compositions.

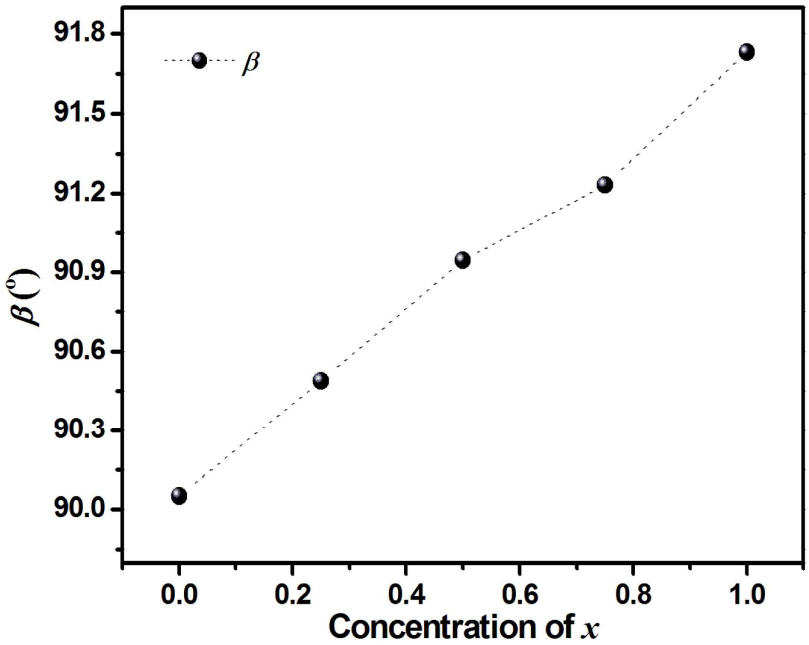

Fig. 3(c). Variation of $d_{(-111)} - d_{(111)}$ in $Ni_{1-x}(Zn_{1/2}Zr_{1/2})_xW_{1-x}Nb_xO_4$ solid solution. (Inset shows the lattice parameter variation and splitting of maximum intense reflection)

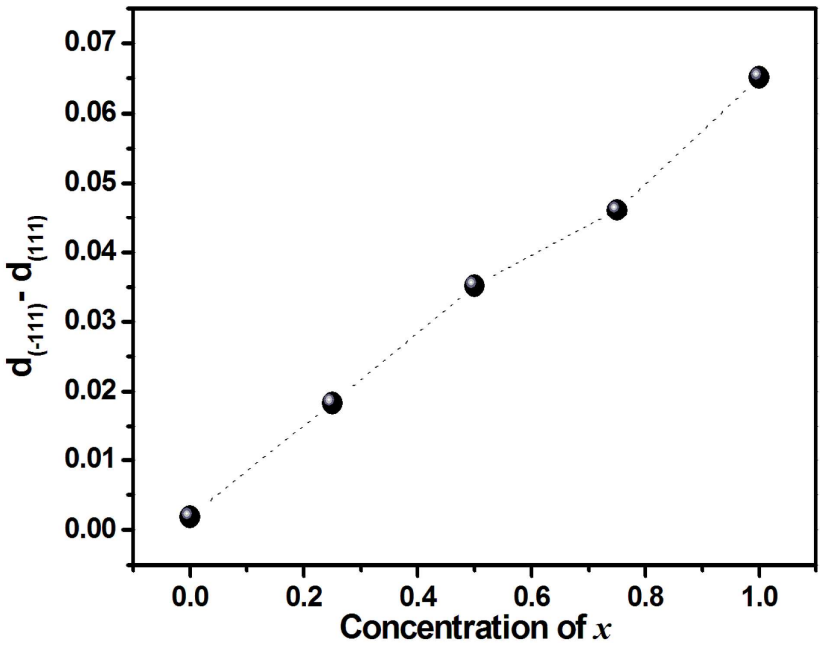

Fig. 4. Crystal structure of $NiWO_4$ composition.

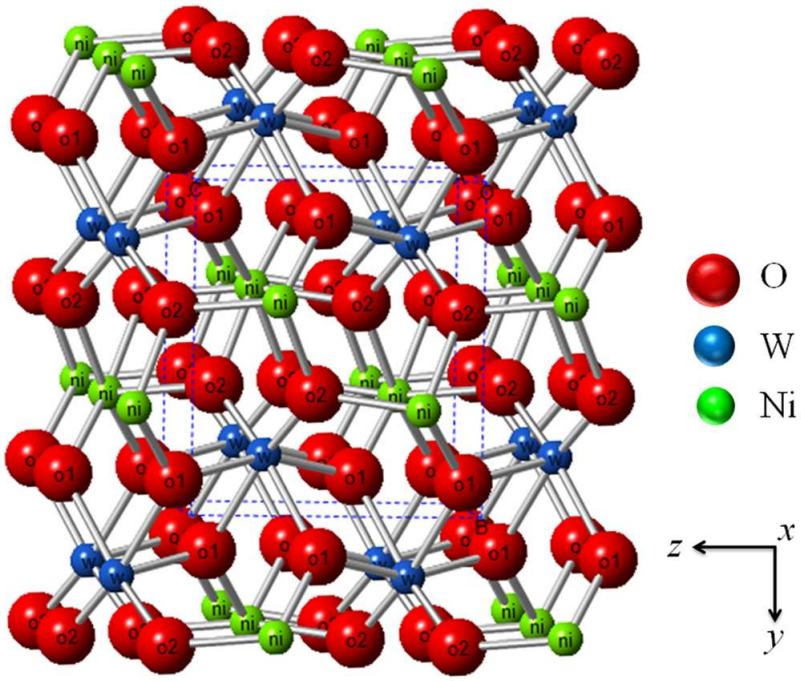

Fig. 5(a). Raman spectra of $Ni_{1-x}(Zn_{1/2}Zr_{1/2})_xW_{1-x}Nb_xO_4$ compositions.

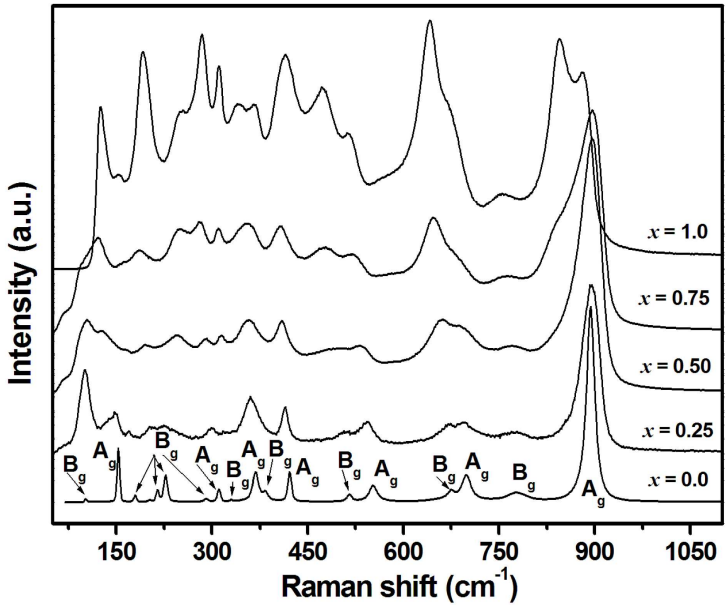

Fig. 5(b). Deconvoluted Raman spectra of $Ni_{1-x}(Zn_{1/2}Zr_{1/2})_xW_{1-x}Nb_xO_4$ compositions.

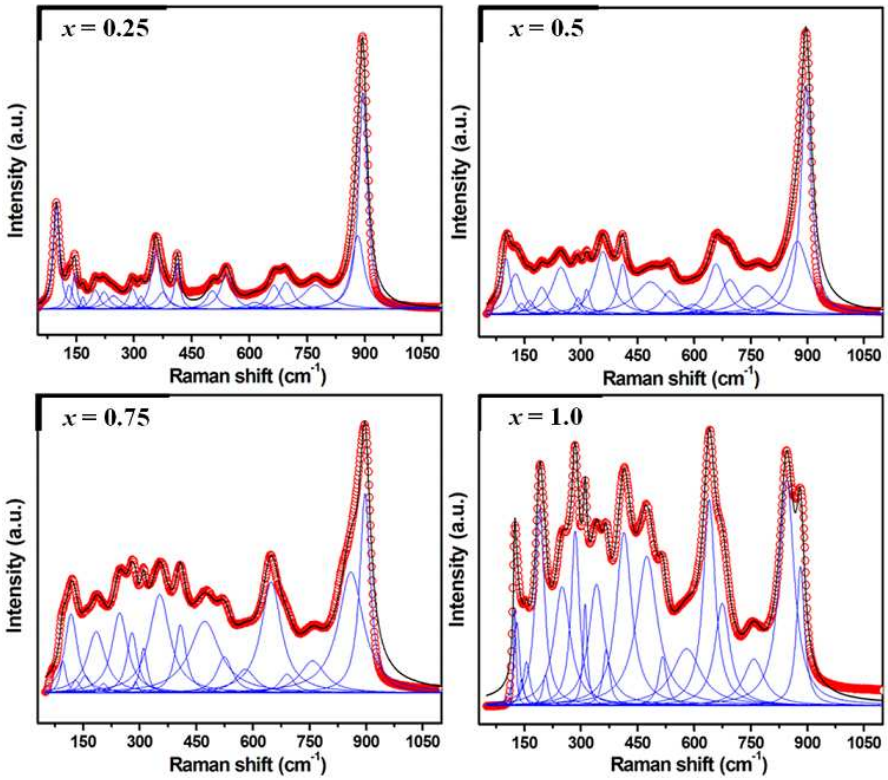

Fig. 6a. High-resolution XPS spectra of (i) Ni (2p), (ii) W (4f) and (iii) O (1s) core levels in $Ni_{1-x}(Zn_{1/2}Zr_{1/2})_xW_{1-x}Nb_xO_4$ compositions.

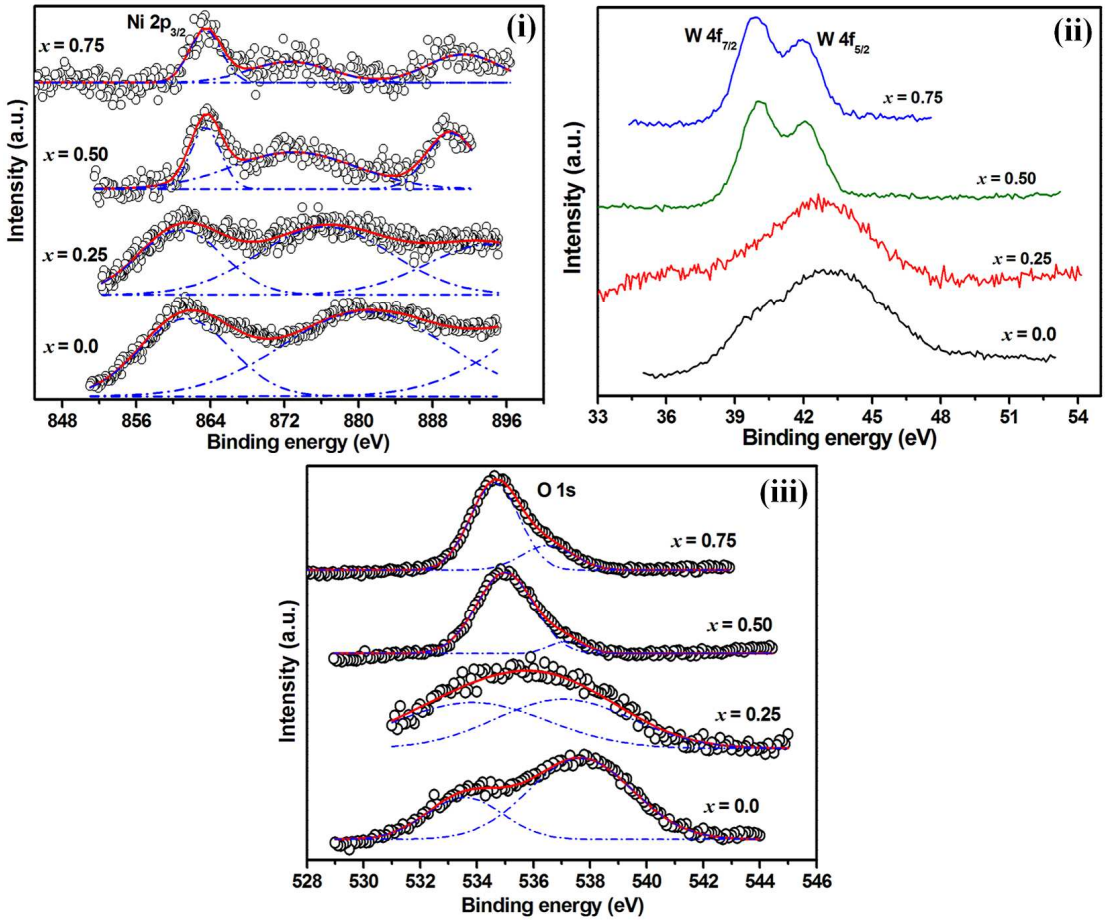

Fig. 6b. High-resolution XPS spectra of (i) Zn (2p), (ii) Zr (3d) and (iii) Nb (3d) core levels in $Ni_{1-x}(Zn_{1/2}Zr_{1/2})_xW_{1-x}Nb_xO_4$ compositions.

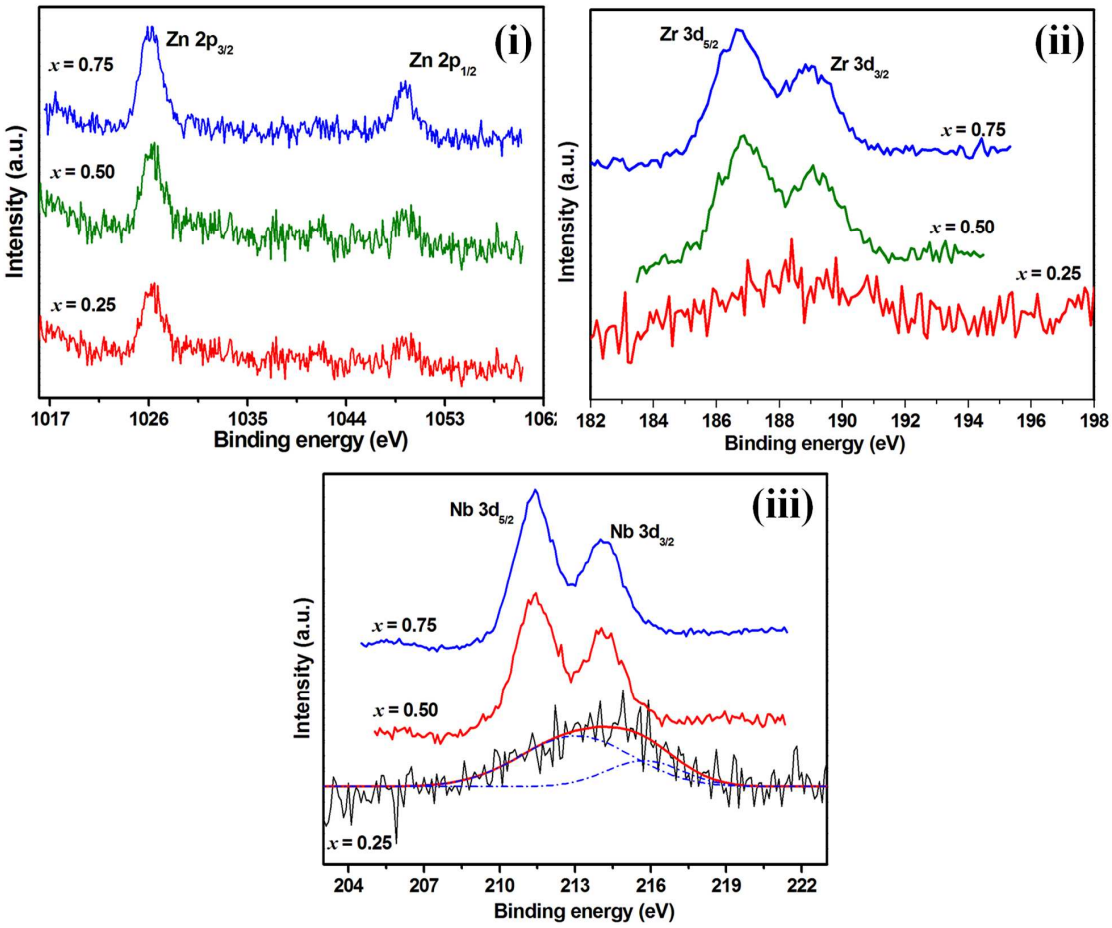

Fig. 7. Scanning electron micrograph of $Ni_{1-x}(Zn_{1/2}Zr_{1/2})_xW_{1-x}Nb_xO_4$ compositions (a) x = 0.0 sintered at 1200 ^oC (b) x = 0.25 sintered at 1250 ^oC (c) x = 0.50 sintered at 1275 ^oC (d) x = 0.75 sintered at 1275 ^oC (e) x = 1.0 sintered at 1300 ^oC.

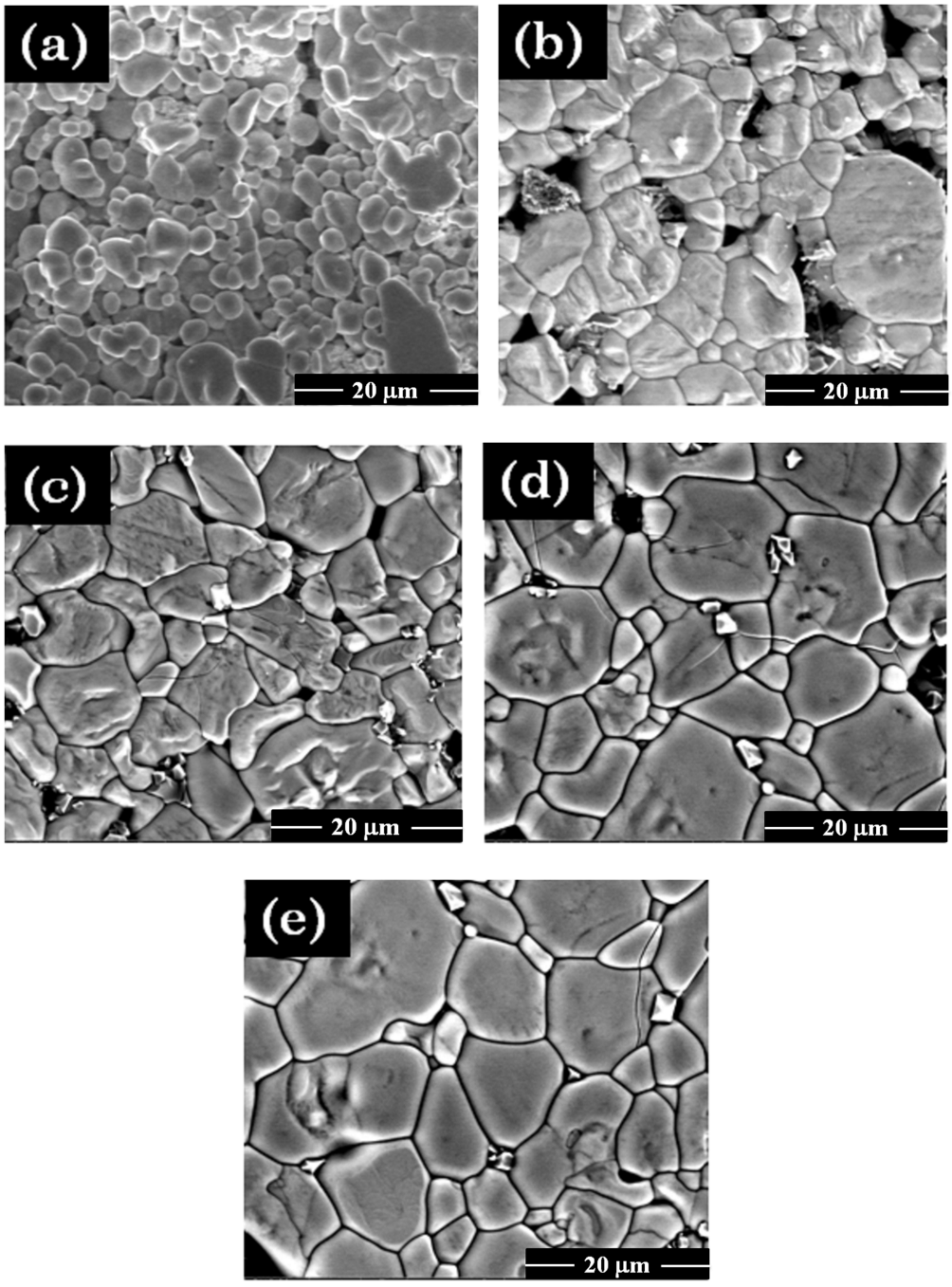

Fig. 8. Variation of dielectric constant and ionic polarizability of $Ni_{1-x}(Zn_{1/2}Zr_{1/2})_xW_{1-x}Nb_xO_4$ compositions.

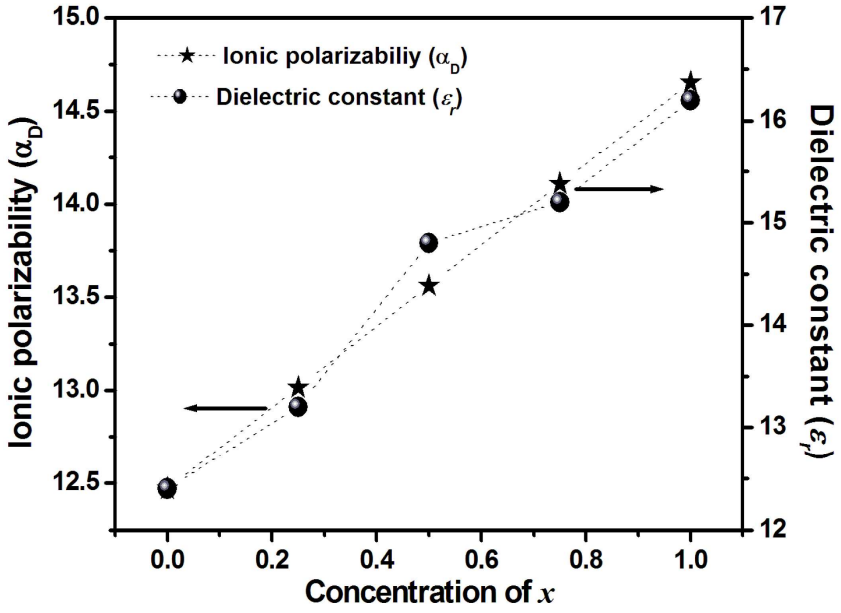

Fig. 9. Variation of quality factor of $Ni_{1-x}(Zn_{1/2}Zr_{1/2})_xW_{1-x}Nb_xO_4$ compositions. (Insets show the variation in (i) AC conductivity and (ii) packing fraction of these compositions with increasing concentration of x)

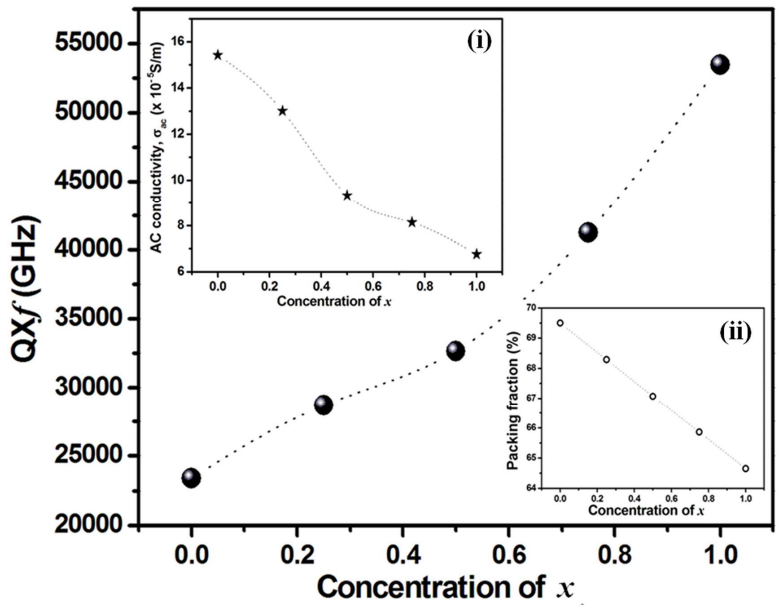

Fig. 10. Correlation among B-site octahedral distortion and temperature coefficient of resonant frequency of $Ni_{1-x}(Zn_{1/2}Zr_{1/2})_xW_{1-x}Nb_xO_4$ compositions.